Binding of Novel Azole-Bridged Dinuclear Platinum(II) Anticancer Drugs to DNA: Insights from Hybrid QM/MM Molecular Dynamics Simulations†

Alessandra Magistrato,*,‡ Paolo Ruggerone,‡,§ Katrin Spiegel,|| Paolo Carloni,‡ and Jan Reedijk⊥

CNR-INFM-Democritos and International School for Advanced Studies, Trieste, Italy, CNR-INFM-SLACS and Department of Physics, University of Cagliari, Monserrato, Cagliari, Italy, Department of Chemistry, University of Pennsylvania, Philadelphia, Pennsylvania 19104, and Leiden Institute of Chemistry, Leiden University, P.O. Box 9502, 2300 RA Leiden, The Netherlands

Received: August 26, 2005

Dinuclear Pt-containing compounds might be used to overcome the intrinsic and acquired cell resistance of widely used anticancer drugs such as cisplatin. Recently, the complexes [{*cis*-Pt(NH_3)$_2$}$_2$(μ-OH)(μ-pz)](NO_3)$_2$ (with pz = pyrazolate) (**1**), [{*cis*-Pt(NH_3)$_2$}$_2$(μ-OH)(μ-1,2,3-ta-N(1),N(2))](NO_3)$_2$ (with ta = 1,2,3-triazolate) (**2**), and the binding of **1** to d(CpTpCpTpG*pG*pTpCpTpCp) have been characterized. Here we provide the structural and electronic properties of the free drugs, of the intermediates of binding to guanine bases, and of the products, by performing DFT calculations. Our results show that in **2** an isomerization of the Pt-coordination sphere from N(2) to N(3) of the triazolate unit determines a thermodynamic stabilization of ∼20 kcal/mol as a consequence of the formation of an allylic structure. In addition, hybrid quantum−classical molecular dynamics simulations of **1** and **2** DNA adducts have shed light on the structural distortions that the drugs induce to the DNA duplex. Our calculations show that the rise and the tilt of the two adjacent guanines are identical in the presence of **1** and **2**, but they markedly increase when **2** binds in the N(1),N(3) fashion. In addition, the drugs do not provoke any kink upon binding to the double-stranded DNA, suggesting that they may act with a mechanism different than that of cisplatin. The accuracy of our calculations is established by a comparison with the NMR data for the corresponding complex with **1**.

1. Introduction

Cisplatin is one of the most widely used anticancer drugs, with particular efficiency in testicular and ovarian cancers (cure rates up to 90% are commonly found).[1−4] The drug targets DNA where it forms primarily 1,2-intrastrand cross-links at the GpG site,[1] causing a kink of 40−80° toward the major groove.[3] Several decades after the discovery of the therapeutic properties of cisplatin, it is still unclear which is the exact role played by this kink either in inducing cell apoptosis either in provoking the response of the DNA repair system.

Severe side effects (such as nausea, ear damage, or vomiting) and intrinsic and acquired cellular resistance have prompted the design of Pt drugs different than cisplatin. Unfortunately, mononuclear, second-generation, Pt drugs (such as carboplatin and oxaliplatin) turned out also to suffer from drug resistance and side effects, and for some tumors they are even less efficient than cisplatin.[1,2,5−7] A viable alternative is the use of dinuclear platinum compounds, which are expected to affect the DNA structure less than first- and second-generation Pt drugs.[8,9] In fact, their structural properties and their flexibility should provide 1,2-intrastrand cross-links, inducing minimal conformational changes to double-stranded (ds) DNA.[8,9] This may overcome the problem of acquired cellular resistance, owing to small induced DNA perturbations and the wide range of pathways leading to inter- and intrastrand linkages.[10,11]

In this respect, azole-bridged dinuclear platinum(II) [{*cis*-Pt(NH_3)$_2$}$_2$(μ-OH)(μ-pz)](NO_3)$_2$ (with pz = pyrazolate) (**1**) and [{*cis*-Pt(NH_3)$_2$}$_2$(μ-OH)(μ-1,2,3-ta-N(1),N(2))](NO_3)$_2$ (with ta = 1,2,3-triazolate) (**2**) (Figure 1)[8,9] have recently shown improved cytotoxicity relative to cisplatin in several tumor cell lines, and they have been shown to circumvent the cross resistance to cisplatin.[10,11]

A mechanism of binding to G-containing double-stranded DNA has been postulated by kinetic and spectroscopic data (Figure 2): A guanine first binds to Pt(1), causing a shift of the OH bridging group to Pt(2), with formation of the intermediate **I1a**/**I2a**. Then, a second guanine replaces OH at the Pt(2) center with formation of the final product **3**/**4**. In addition, after the formation of **I2a** an isomerization mechanism has been observed for **2** in which the Pt(2) atom migrates from N(2) to N(3) of the triazolate ligand (**I2b**).[10,11] This isomerization occurs exclusively for **2**, and it is not observed experimentally after the formation of complex **4**.[10,11] When the distance between the two metal centers is increased, this isomerization leads to the formation of a variety of inter- and intrastrand cross-links, which may be a key factor for the high cytotoxicity of the drugs.[10,11] The NMR structure of **1** with d(CpTpCpTpG*pG*pTpCpTpCp) has showed that the drug causes only minimal local distortions to the DNA structure.[1,12]

In the present article, we have performed a structural and electronic study (based on density functional theory (DFT)) of the two drugs, of the intermediates of binding to guanine bases, and of the products to characterize structural and electronic

† Part of the special issue "Michael L. Klein Festschrift".

* Author to whom correspondence should be addressed. E-mail: alema@sissa.it.

‡ CNR-INFM-Democritos and International School for Advanced Studies.

§ CNR-INFM-SLACS and University of Cagliari.

|| University of Pennsylvania.

⊥ Leiden University.

10.1021/jp054828p CCC: $33.50
Published on Web 12/08/2005

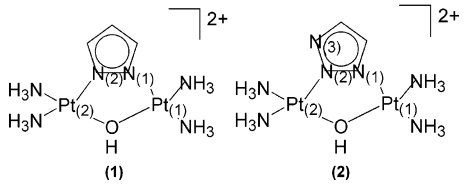

Figure 1. [{*cis*-Pt(NH_3)$_2$}$_2$(μ-OH)(μ-pz)]$^{2+}$ (with pz = pyrazolate) (**1**) and [{*cis*-Pt(NH_3)$_2$}$_2$(μ-OH)(μ-1,2,3-ta-N(1),N(2))]$^{2+}$ (with ta = 1,2,3-triazolate) (**2**).

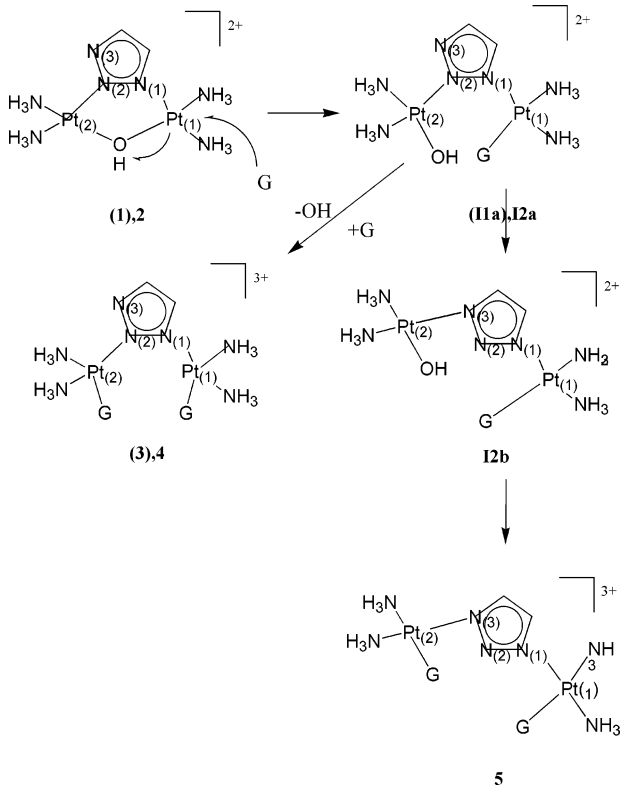

Figure 2. Mechansim of binding of the azole-bridged diplatinum drugs to guanine bases. The mechanism is shown for **2**, and in parentheses are indicated the corresponding compounds of **1**. These complexes are equivalent to the ones depicted in this picture, with N(3) replaced by a C(3)−H group.

differences that may explain the reactivity and the mechanism of action of these drugs.

To simulate the drug−DNA adducts we have adopted a hybrid quantum−classical (QM/MM) approach.[13] Since the Pt-coordination geometry depends dramatically on the electronic structure of the transition metal,[14] it is very difficult to describe the coordination geometry of Pt complexes accurately by effective potentials. However, by treating at the QM level the two platinum centers and its coordination ligands we can reliably describe the coordination geometry of the metallic centers, and by describing the DNA (and the solvent) at the MM level, we can observe structural distortions induced by the diplatinated drug on the ds DNA. This allows us to take into account the mechanical and the electrostatic role of the DNA and the solvent at the atomistic level.

Some of us have already successfully applied a QM/MM approach to the study of a cisplatin−DNA adduct,[15] and we employ it here to simulate **1** and **2** in complex with a ds DNA decamer, considering for the latter drug both the N(1),N(2) and the N(1),N(3) binding modes.

A detailed understanding of the structural and electronic properties of these drugs and these drug−DNA adducts might elucidate the origin of their different cytotoxic activities and might be of help in the design of more specific anticancer compounds.

2. Computational Details

2.1. DFT Calculations. The calculations on **1** and **2** (Figure 1) are based on the X-ray structure of **2**[8] (i.e., for **1** we have manually replaced N(3) with a C(3)−H group). Those on [{*cis*-Pt(NH_3)$_2$}$_2$(G−N(7))$_2$(μ-pz)]$^{3+}$ (**3**), [{*cis*-Pt(NH_3)$_2$}$_2$(G−N(7))$_2$(μ-1,2,3-ta-N(1),N(2))]$^{3+}$ (**4**), and [{*cis*-Pt(NH_3)$_2$}$_2$(G−N(7))$_2$(μ-1,2,3-ta-N(1),N(3)]$^{3+}$ (**5**) are based on the X-ray structure of [{*cis*-Pt(NH_3)$_2$}$_2$(9EtG−N(7))$_2$(μ-pz)]$^{3+}$ [9] (Figures 2 and 3) in which we have removed the ethyl group, and we have generated the triazolate ring manually for **4** and **5**. In addition, we have generated the intermediates of the binding process by replacing one guanine with a hydroxyl ligand [{*cis*-Pt(NH_3)$_2$}$_2$-(G−N(7))(OH)(μ-pz)]$^{2+}$ (**I1a**), [{*cis*-Pt(NH_3)$_2$}$_2$(G−N(7))(OH)-(μ-1,2,3-ta-N(1),N(2])$^{2+}$ (**I2a**), and [{*cis*-Pt(NH_3)$_2$}$_2$(G−N(7))-(OH)(μ-1,2,3-ta-N(1),N(3))]$^{2+}$ (**I2b**). Finally, to discriminate between the steric and the electronic influence of the ligands on the isomerization step, we have also relaxed the structure of [{*cis*-Pt(NH_3)$_2$}$_2$(G−N(7))(NH_3)(μ-1,2,3-ta-N(1),N(2))]$^{3+}$ and [{*cis*-Pt(NH_3)$_2$}$_2$(G−N(7))(NH_3)(μ-1,2,3-ta-N(1),N(3))]$^{3+}$ (**I3a** and **I3b**) in which the hydroxyl ligand has been replaced with an ammonia molecule.

The calculations have been performed using the program CPMD with a plane wave (PW) basis set up to an energy cutoff of 70 Ry.[16] Core−valence interactions were described using norm-conserving pseudopotentials of the Martins−Troullier type.[17] Integration of the nonlocal parts of the pseudopotential was obtained via the Kleinman−Bylander scheme[18] for all of the atoms except platinum, for which a Gauss−Hermite numerical integration scheme was used. The gradient-corrected Becke exchange functional and the Lee−Yang−Parr correlation functional (BLYP) were used.[19,20] Periodic boundary conditions were applied, and we have used orthorhombic cells of the edges of a = 10.0 Å, b = 15.5 Å, and c = 17.0 Å for **1** and **2**, of a = 17.5 Å, b = 14.0 Å, and c = 14.0 Å for all of the intermediates, and of a = 19.0 Å, b = 16.5 Å, and c = 16.5 Å for the products. Isolated system conditions[21] were applied.

2.2. Classical Molecular Dynamics Calculations. The structures of [{*cis*-Pt(NH_3)$_2$}$_2$(d(GN(7)*GN(7)*)(μ-pz)]·(d(CpTpCpTpG*pG*pTpCpTpCp)) (**A**), [{*cis*-Pt(NH_3)$_2$}$_2$(d(GN(7)*GN(7)*)(μ-1,2,3-ta-N(1),N(2))]·(d(CpTpCpTpG*pG*pTpCpTpCp)) (**B**), [{*cis*-Pt(NH_3)$_2$}$_2$(d(GN(7)*GN(7)*)(μ-1,2,3-ta-N(1),N(3))]·(d(CpTpCpTpG*pG*pTpCpTpCp)) (**C**), and (d-(CpTpCpTpG*pG*pTpCpTpCp)) (**D**) were considered.

For **A** we have chosen the NMR structure as the starting model, for **B** and **C** we have manually docked **2** (in the N(1),N-(2) and N(1),N(3) coordination modes) into the NMR structure, and in **D** we have constructed a decamer with the same sequence of the NMR structure using the xleap module of the AMBER package.[22,23] The drug−DNA complexes were inserted in a water box of 10 Å. Ten potassium counterions were added to neutralize their charge. The total systems contained ∼19 200 atoms (∼6100 water molecules).

The AMBER parm98 force field[24,25] was adopted for the oligonucleotide and the potassium counterions. The TIP3P model[26] was used for water. The parametrization of Herman et al.[27] for bonds and angles was used along with harmonic constraints of 5 kcal/(mol Å^2) on the atomic positions for the platinated moiety, namely, [{*cis*-Pt(NH_3)$_2$}$_2$(d(GN(7)*GN(7)*)-(μ-pz-N(1),N(2))] for **A**, [{*cis*-Pt(NH_3)$_2$}$_2$(d(GN(7)*GN(7)*)-(μ-1,2,3-ta-N(1),N(2))] for **B**, and [{*cis*-Pt(NH_3)$_2$}$_2$(d(GN(7)-*GN(7)*)(μ-1,2,3-ta-N(1),N(3))] for **C**.

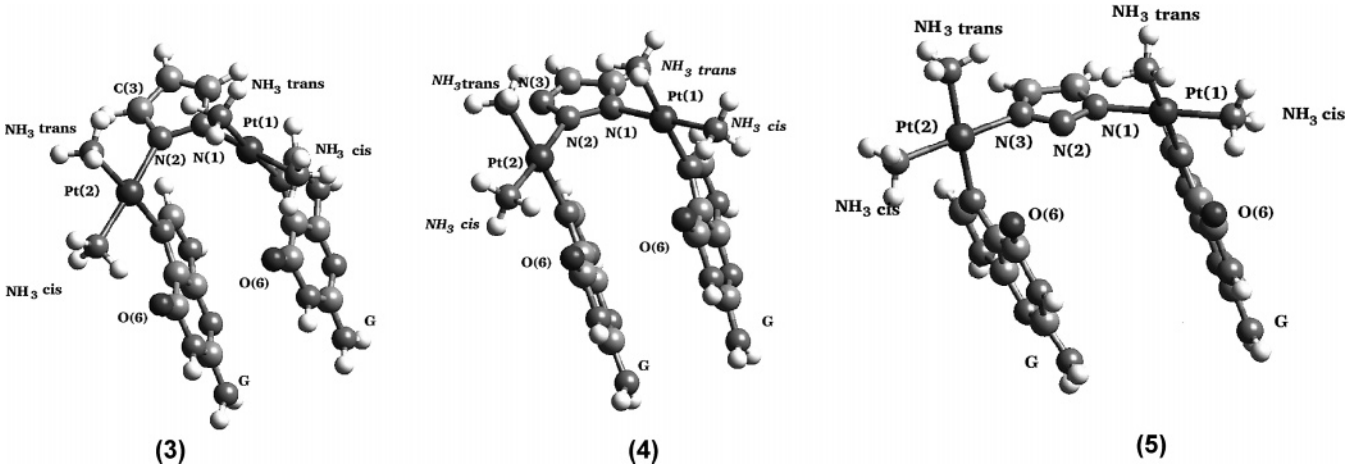

Figure 3. [{*cis*-Pt$(NH_3)_2$}$_2$$(G)_2$($\mu$-pz)]$^{3+}$ (with pz = pyrazolate) (**3**), [{*cis*-Pt$(NH_3)_2$}$_2$$(G)_2$($\mu$-1,2,3-ta-N(1),N(2))]$^{3+}$ (**4**), and [{*cis*-Pt$(NH_3)_2$}$_2$$(G)_2$-($\mu$-1,2,3-ta-N(1),N(3))]$^{3+}$ (with ta = 1,2,3-triazolate) (**5**).

These constraints have been applied to keep the platinated moiety as close as possible to the experimental structure, preventing a biasing of the initial QM/MM structure. In fact, due to the rather crude parameters of the Pt moiety, our classical molecular dynamics (MD) simulations are performed only to provide an equilibrated starting structure for QM/MM simulations.

Electrostatics were evaluated with the particle mesh Ewald (PME) method.[28] A cutoff of 10 Å was used for the van der Waals interactions and the real part of the electrostatic interactions. A time step of 1.5 fs was applied. Room-temperature simulations were achieved by coupling the systems to a Berendsen thermostat.[29] The initial structures were relaxed by short steepest descent minimization runs of 1000 steps. 100 ps of MD simulation at constant volume was performed during which the system was heated to 300 K. A MD simulation of 2 ns at constant pressure (1 atm) and temperature (300 K) was then performed. The MD simulations were carried out with the AMBER7 program package.[22,23]

2.3. QM/MM Calculations. The CPMD program[16] is combined with classical molecular dynamics (MD), based on both the GROMOS96[30] and the AMBER force fields,[28,29] through the interface developed by Rothlisberger et al.[13,31]

The **A**, **B**, and **C** classically equilibrated MD structures were taken as the starting points of QM/MM simulations. These systems were divided into two regions (Figure 4). The first region, treated at the quantum mechanical (QM) level, comprises the two platinum metal centers, the pyrazolate/triazolate bridging unit, the four ammonia ligands, and the two guanine bases (G5 and G6). The guanines have been cut at C(1′), and the valence of the terminal carbon atoms has been saturated by the addition of capping hydrogen atoms (63 QM atoms). The remaining part of the system, including waters and counterions, has been modeled at the molecular mechanical (MM) level (∼19 200 atoms, ∼6100 water molecules).

The QM region was treated at the DFT level with the same computational setup described in section 2.1, while the MM region was described with the AMBER force field.[24,25] The electrostatic interactions between QM and MM atoms were calculated using a hierarchical scheme.[13] In this approach, the short-range electrostatic interactions between the QM and MM part were taken explicitly into account within a sphere of radius 5.3 Å around every QM atom using an appropriately modified Coulomb potential that avoids electron spillout. Beyond this first shell and within 10.6 Å, the electrostatic interactions were calculated using the D-RESP charges[31] for the QM atoms. In the outermost region, a multipolar expansion scheme was employed. This hierarchical method is fully Hamiltonian, and it ensures high accuracy in the core region and efficient computation in the region further away from the QM part.

To relax the systems we have initially performed 1000 steps of simulated annealing, and then the systems were slowly heated to 300 K. A time step of 0.096 fs was used with a fictitious electronic mass of 600 a.u. NVT simulations were carried out by coupling the systems to a Nose−Hoover thermostat.[32,33] Periodic boundary conditions were applied using for the QM part an orthorhombic box with dimensions a = 17.5 Å, b = 16.7 Å, and c = 16.7 Å for the three models. Periodic images have been decoupled.[21] For the classical part we have used an orthorhombic box of the edges of a = 57.7 Å, b = 54.5 Å, and c = 60.5 Å.

2.4. Structural and Electronic Analysis. Structural parameters of DNA (helix bending, angle between base pairs,[34] rise, twist, roll, tilt, and propeller twist angles) are defined according to the EMBO Workshop on DNA Curvature and Bending[35] and were calculated with the program Curves.[36]

The radial distribution function and root-mean-square deviation were calculated with the ptraj module of AMBER.[22,23]

Boys orbitals were calculated,[37] and on the basis of their localization we have analyzed the bond ionicities. The bond ionicity of A−B (BI_{AB}) was calculated as in ref 38, namely, $BI_{AB} = (|\vec{\mathbf{d}}_A|\cos\theta)/|\mathbf{d}_{AB}|$ where $\vec{\mathbf{d}}_A$ is the position vector between atom A and the Boys orbital along the AB bond, $\vec{\mathbf{d}}_{AB}$ is the position vector of the bond between A and B, and θ is the angle between the vectors. BIs identify electron lone pairs and provide an estimation of ionicity of chemical bonds.[38]

3. Results and Discussion

3.1. Complexes 1−2 and Their Derivatives. The geometries of complexes **1** and **2** (Figure 1) were optimized by using DFT calculations. The calculated geometry of **2** agrees fairly well with the corresponding X-ray data (Δd = 0.07 Å; 3% relative error, Table 1). The observed error is due to the BLYP exchange correlation functional that is known to slightly overestimate the bond lengths.[15,39] The coordination of the metal ions of **1** and **2** is essentially square-planar, and it is not altered by the presence of either the pyrazolate or the triazolate ring. This is confirmed by the bond ionicities (Table 2).[37,38] Trivially, the only difference is observed in the pyrazolate and in the triazolate rings in which N(1)−N(2) and C(3)/N(3)−N(2) bonds are slightly longer in **1** than those in **2** (1.39 and 1.37 Å and 1.37 and 1.33 Å in **1** and

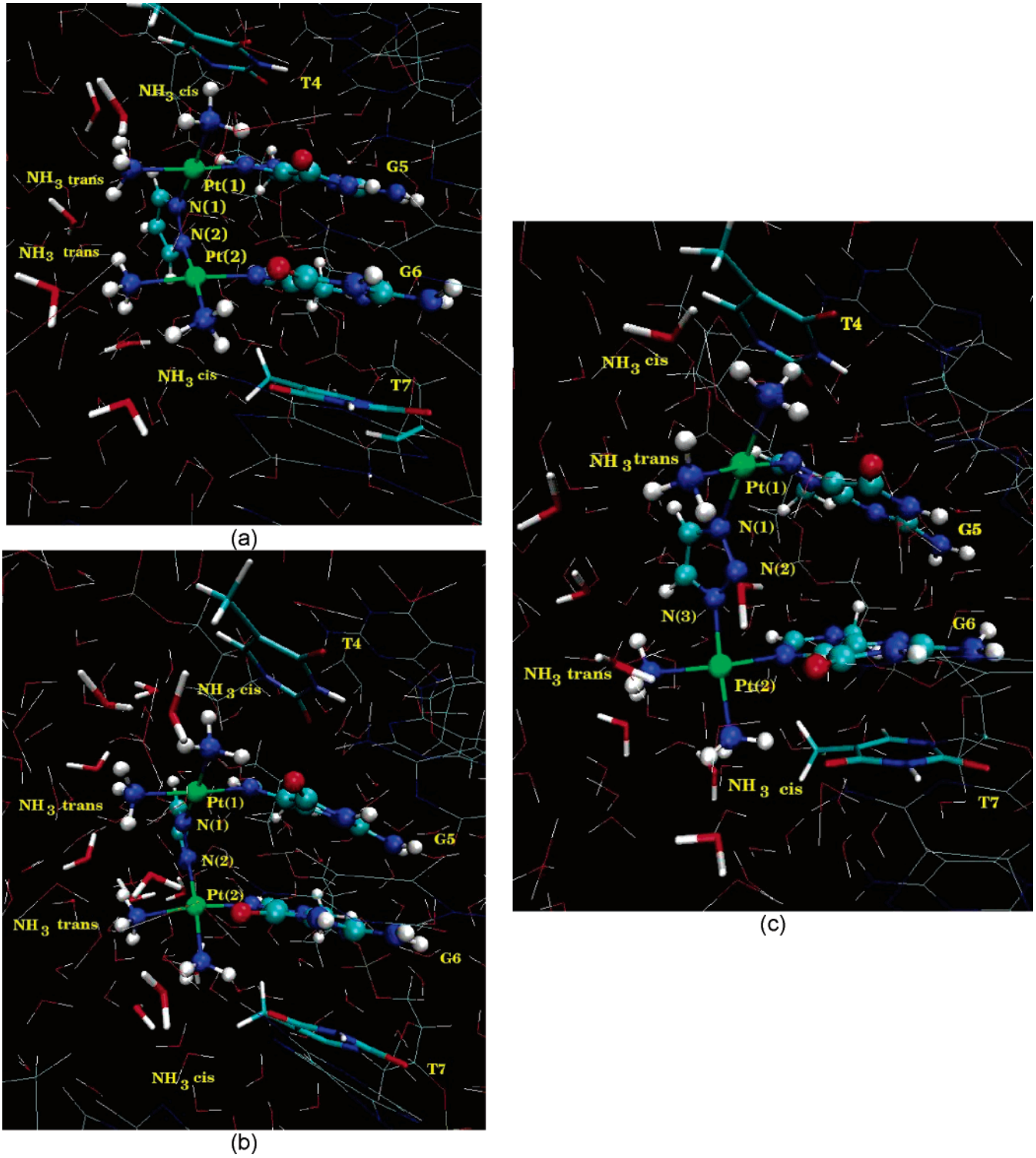

Figure 4. (a) Average structure for model **A**, (b) **B**, and (c) **C**. Atoms depicted by a ball-and-stick model belong to the QM region, the remaining atoms and the solvent belong to the MM region. T4, T7, and water molecules forming hydrogen bonds with the NH_3 ligands are depicted by sticks.

2, respectively) and correspond to $BI_{N(1)-N(2)} = 0.50$ for both **1** and **2** and $BI_{C(3)/N(3)-N(2)} = 0.64$, 0.66 and 0.59, 0.60 for **1** and **2**, respectively. The latter BIs indicate a partial double bond character that for the pyrazolate ring is more ionic. The distance between the two platinum atoms is 3.5/3.6 Å. This value is very close to the typical rise of the base pairs in canonical B-DNA, suggesting that the drug will not cause large distortions upon binding to the DNA.

Replacing the OH ligand with two guanines (**3** and **4**, Figures 2 and 3) does not affect the square-planar coordination geometry. The only significant difference with **1** and **2** is an increase in the distance between the two Pt centers by ~0.4 Å (Table 1). This corresponds to an average distance between the centers of the two guanine rings of 3.73 Å from the X-ray[9] structure versus 4.09 and 3.97 Å for **3** and **4**, respectively.[40] The small increment of 0.2−0.3 Å might be due to the lack of dispersion interactions between the two π-stacked guanines.[41] The hydrogen bonds between $NH_{3\,cis}$ (i.e., cis with respect to the guanine ring) and O(6)@G (1.99 and 1.71 Å, and 2.23 and 2.01 Å for **3** and **4**, respectively) stabilize the complexes.

TABLE 1: Selected Bond Lengths[a]

	X-ray (2)	1	2		X-ray (3)	3	4	5		I1a	I2a	I2b		I3a	I3b
Pt(1)···Pt(2)	3.44	3.53	3.58	Pt(1)···Pt(2)	3.70	3.99	3.94	5.93	Pt(1)···Pt(2)	3.91	3.93	5.96	Pt(1)···Pt(2)	3.97	5.98
Pt(1)−OH	2.02	2.07	2.08	Pt(1)−N(7)G	2.05	2.06	2.05	2.05	Pt(1)−N(7)G	2.06	2.06	2.06	Pt(1)−N(7)G	2.06	2.06
Pt(1)−N(1)	1.99	1.98	2.02	Pt(1)−N(1)	2.00	2.05	2.05	2.03	Pt(1)−N(1)	2.04	2.04	2.04	Pt(1)−N(1)	2.06	2.06
Pt(1)−$NH_{3\ trans}$	2.04	2.10	2.11	Pt(1)−$NH_{3\ trans}$	2.03	2.10	2.10	2.11	Pt(1)−$NH_{3\ trans}$	2.10	2.10	2.09	Pt(1)−$NH_{3\ trans}$	2.08	2.10
Pt(1)−N(2)$H_{3\ cis}$	2.03	2.07	2.09	Pt(1)−$NH_{3\ cis}$	2.09	2.10	2.10	2.05	Pt(1)−$NH_{3\ cis}$	2.10	2.09	2.09	Pt(1)−$NH_{3\ cis}$	2.10	2.08
Pt(2)−OH	2.02	2.08	2.08	Pt(2)−N(7)G	2.06	2.06	2.06	2.05	Pt(2)−OH	2.00	2.00	1.99	Pt(2)−$NH_{3\ trans}$	2.08	2.12
Pt(2)−N(2)	1.98	2.02	1.99	Pt(2)−N(2)	2.01	2.05	2.04		Pt(2)−N(2)	2.03	2.03		Pt(2)−N(2)	2.03	
Pt(2)−N(3)				Pt(2)−N(3)				2.04	Pt(2)−N(3)			2.03	Pt(2)−N(3)		2.03
Pt(2)−$NH_{3\ trans}$	2.04	2.11	2.11	Pt(2)−$NH_{3\ trans}$	2.01	2.10	2.10	2.09	Pt(2)−$NH_{3\ trans}$	2.14	2.13	2.14	Pt(2)−$NH_{3\ trans}$	2.09	2.09
Pt(1)−N(1)$H_{3\ cis}$	2.03	2.10	2.10	Pt(1)−$NH_{3\ cis}$	2.06	2.09	2.09	2.09	Pt(1)−$NH_{3\ cis}$	2.09	2.08	2.09	Pt(1)−$NH_{3\ cis}$	2.11	2.12
N(1)−N(2)	1.35	1.39	1.37	N(1)−N(2)	1.99	1.40	1.39	1.35	N(1)−N(2)	1.39	1.38	1.35	N(1)−N(2)	1.39	1.35
N(2)−N(3)	1.33		1.33	N(2)−N(3)			1.33	1.35	N(2)−N(3)		1.33	1.35	N(2)−N(3)	1.33	1.35
N(2)−C(3)		1.37		N(2)−C(3)	1.35	1.37			N(2)−C(3)	1.36			N(2)−C(3)		

[a] Selected bond lengths (Å) are given for $[\{cis\text{-}Pt(NH_3)_2\}_2(\mu\text{-}OH)(\mu\text{-}pz)]^{2+}$ (with pz = pyrazolate) (**1**), $[\{cis\text{-}Pt(NH_3)_2\}_2(\mu\text{-}OH)(\mu\text{-}1,2,3\text{-ta-}N(1),N(2)))]^{2+}$ with ta = 1,2,3 triazolate) (**2**), $[\{cis\text{-}Pt(NH_3)_2\}_2(GN(7))_2(\mu\text{-}pz)]^{3+}$ (**3**) $[\{cis\text{-}Pt(NH_3)_2\}_2(GN(7))_2(\mu\text{-}1,2,3\text{-ta-}N(1),N(2))]^{3+}$ (**4**), and $[\{cis\text{-}Pt(NH_3)_2\}_2(GN(7))_2(\mu\text{-}1,2,3\text{-ta-}N(1),N(3))]^{3+}$ (**5**). The trans label for **1** and **2** indicates trans to the OH ligand, while for **3**, **4**, and **5** the trans label indicates trans to the guanine bases. Selected bond lengths are also given for $[\{cis\text{-}Pt(NH_3)_2\}_2(GN(7))OH(\mu\text{-}pz]^{2+}$ (**I1a**), $[\{cis\text{-}Pt(NH_3)_2\}_2(GN(7))OH(\mu\text{-}1,2,3\text{-ta-}N(1),N(2))]^{2+}$ (**I2a**), $[\{cis\text{-}Pt(NH_3)_2\}_2(GN(7))OH(\mu\text{-}1,2,3\text{-ta-}N(1),N(3))]^{2+}$ (**I2b**), $[\{cis\text{-}Pt(NH_3)_2\}_2(GN(7))(NH_3)(\mu\text{-}1,2,3\text{-ta-}N(1),N(2))]^{3+}$ (**I3a**), and $[\{cis\text{-}Pt(NH_3)_2\}_2(GN(7))(NH_3)(\mu\text{-}1,2,3\text{-ta-}N(1),N(3))]^{3+}$ (**I3b**).The trans label refers to the OH and the NH_3 ligand for **I1a**, **I2a**, and **I2b** and **I3a** and **I3b**, respectively. The atom labeling scheme is depicted in Figures 1, 2, and 3.

TABLE 2: Bond Ionicities[37,38] of 1−5 and the Reaction Intermediates I1a, I2a, I2b, I3a, and I3b from Figure 2[a]

	1	2		3	4	5		I1a	I2a	I2b		I3a	I3b
Pt(1)−OH	0.76	0.76	Pt(1)−N(7)G	0.71	0.70	0.71	Pt(1)−N(7)G	0.72	0.72	0.72	Pt(1)−N(7)G	0.72	0.72
Pt(1)−N(1)	0.71	0.71	Pt(1)−N(1)	0.71	0.72	0.70	Pt(1)−N(1)	0.70	0.71	0.71	Pt(1)−N(1)	0.72	0.72
Pt(1)−$NH_{3\ trans}$	0.74	0.72	Pt(1)−$NH_{3\ trans}$	0.72	0.73	0.73	Pt(1)−$NH_{3\ trans}$	0.73	0.73	0.73	Pt(1)−$NH_{3\ trans}$	0.73	0.73
Pt(1)−$NH_{3\ cis}$	0.72	0.71	Pt(1)−$NH_{3\ cis}$	0.73	0.72	0.71	Pt(1)−$NH_{3\ cis}$	0.72	0.72	0.71	Pt(1)−$NH_{3\ cis}$	0.71	0.70
Pt(2)−OH	0.76	0.77	Pt(2)−N(7)G	0.71	0.71	0.70	Pt(2)−OH	0.70	0.70	0.69	Pt(2)−$NH_{3\ trans}$	0.73	0.73
Pt(2)−N(2)	0.70	0.70	Pt(2)−N(2)	0.71	0.71		Pt(2)−N(2)	0.72	0.71		Pt(2)−N(2)	0.70	
Pt(2)−N(3)			Pt(2)−N(3)			0.72	Pt(2)−N(3)			0.72	Pt(2)−N(3)		0.70
Pt(2)−$NH_{3\ trans}$	0.72	0.71	Pt(2)−$NH_{3\ trans}$	0.73	0.73	0.73	Pt(2)−$NH_{3\ trans}$	0.75	0.75	0.75	Pt(2)−$NH_{3\ trans}$	0.73	0.73
Pt(2)−$NH_{3\ cis}$	0.74	0.74	Pt(2)−$NH_{3\ cis}$	0.72	0.72	0.72	Pt(2)−$NH_{3\ cis}$	0.73	0.73	0.74	Pt(2)−$NH_{3\ cis}$	0.73	0.72
N(1)−N(2)	0.50	0.50	N(1)−N(2)	0.50	0.50	0.34	N(1)−N(2)	0.50	0.51	0.34	N(1)−N(2)	0.50	0.39
						0.41				0.41			0.40
N(3)−N(2)		0.59	N(3)−N(2)		0.67	0.38	N(3)−N(2)		0.54	0.40	N(3)−N(2)	0.60	0.37
		0.60			0.60	0.39			0.55	0.40		0.63	0.39
C(3)−N(2)	0.64		C(3)−N(2)	0.64			C(3)−N(2)	0.61			C(3)−N(2)		
	0.66			0.67				0.62					

[a] For the calculation of the bond ionicity, see section 2.4.

Interestingly, shifting the Pt(2) center of **4,** along with its coordination ligands, from N(2) to N(3) (**5,** Figures 2 and 3), does not affect significantly the platinum ion coordination. The only relevant difference is in the length and in the ionicity of the N(1)−N(2) and N(2)−N(3) bonds: d(N(1)−N(2)) = 1.39 Å, d(N(2)−N(3)) = 1.33 Å for **4** and d(N(1)−N(2)) = d(N(2)−N(3)) = 1.35 Å for **5**; $BI_{N(1)-N(2)}$ = 0.50, $BI_{N(3)-N(2)}$ = 0.67 and 0.60 for **4,** $BI_{N(1)-N(2)}$ = 0.34 and 0.41 and $BI_{N(3)-N(2)}$ = 0.36 and 0.39 for **5**. (In addition, in **5** a lone pair is localized on N(2).[42]) The identical length and ionicity of the N(1)−N(2) and N(2)−N(3) bonds of **5** suggest the formation of an allylic structure in which the electronic density is delocalized over three nitrogen atoms. A visual inspection of the Kohn−Sham orbitals confirms this hypothesis. In fact, an orbital connecting the three nitrogen atoms is observed (HOMO-15) along with an orbital indicating an electronic correlation between the two metal centers and the allylic structure (HOMO-20) (Figures 5a and 5b, respectively). Similar molecular orbitals are not present in **4**.

The shift of Pt(2) to another donor site of the ligand determines a thermodynamic stabilization of ∼20 kcal/mol of **5** with respect to **4**.

To gain insights into the mechanism of binding to the DNA we focus our attention also on the reaction intermediates. We have simulated the proposed intermediates of the binding in which the hydroxyl ligand replaces the Pt(2)@G of **3**−**5** (Figure 2).[10,11] These intermediates feature both the pyrazolate (**I1a**) and the triazolate bridging unit, for the latter considering the two possible structural isomers, i.e., without and with Pt(2) translation along the bridging unit (**I2a** and **I2b,** respectively).

The Pt(1) coordination sphere is unchanged in **I1a** and in both **I2a** and **I2b**, while at the second coordination center we observe a strengthening of the Pt(2)−OH bond by −0.06 Å (with respect to Pt(2)−N(7)G) and consequently an increase by +0.04 Å of the Pt(2)−$NH_{3\ trans}$. A relevant electronic rearrangement of the bridging unit occurs in the presence of the hydroxyl ligand. In fact, the bond ionicity of the C(3)/N(3)−N(2) bonds decreases by $\Delta BI_{C(3)-N(2)}$ = −0.05 and −0.03 and $\Delta BI_{N(3)-N(2)}$ = −0.12 and −0.06 for **I1a** and **I2a** with respect to **3** and **4**, respectively.[42] This indicates that the electron density moves far away from the hydroxyl ligand. In fact, the negatively charged hydroxyl group reduces the electronic density subtracted from the bridging ring, resulting in a more covalent C(3)/N(3)−N(2) double bond character (Table 2). Consistently, after the N(2),N(3) isomerization of the Pt(2) coordination sphere we observe $\Delta BI_{N(3)-N(2)}$ = +0.05 and +0.01 for **I2b** with respect to **5**, always resulting in a more covalent double bond character. Since the Pt(2) moiety now coordinates to N(3), the electronic density is shifted toward N(2). This electronic reorganization determines an overall thermodynamic stabilization of approximately −10 kcal/mol of **I2b** relative to **I2a.** This trend is further confirmed by a structural and electronic analysis of

TABLE 3: Selected Bond Lengths (Å) for QM/MM Models of the Drug−DNA Adducts[a]

bond distances (Å)	NMR	A	B	C
Pt(1)···Pt(2)	3.82	3.8 ± 0.1	4.1 ± 0.1	5.9 ± 0.1
Pt(1)−N(7)G5	2.03	2.08 ± 0.05	2.08 ± 0.05	2.06 ± 0.04
Pt(1)−N(1)	2.02	2.05 ± 0.04	2.06 ± 0.04	2.04 ± 0.04
Pt(1)−$NH_{3\ trans}$	2.04	2.07 ± 0.03	2.08 ± 0.03	2.08 ± 0.05
Pt(1)−$NH_{3\ cis}$	2.04	2.08 ± 0.03	2.07 ± 0.04	2.08 ± 0.04
Pt(2)−N(7)G6	2.02	2.07 ± 0.05	2.06 ± 0.05	2.05 ± 0.04
Pt(2)−N(2)	2.02	2.06 ± 0.05	2.07 ± 0.06	
Pt(2)−N(3)				2.03 ± 0.04
Pt(2)−$NH_{3\ trans}$	2.03	2.08 ± 0.03	2.08 ± 0.04	2.08 ± 0.04
Pt(2)−$NH_{3\ cis}$	2.04	2.08 ± 0.04	2.07 ± 0.03	2.10 ± 0.07
N(1)−N(2)	1.37	1.39 ± 0.02	1.38 ± 0.02	1.35 ± 0.02
N(2)−N(3)			1.34 ± 0.02	1.35 ± 0.02
N(2)−C(3)	1.37	1.36 ± 0.01		

[a] In **A** the two platinum atoms bind to the two nitrogen atoms of the pyrazolate ligand; in **B** and **C**, they bind to N(1),N(2) and to N(1),N(3) of the triazolate, respectively. The trans or cis labels indicate the NH_3 cis or trans to the guanine bases. The atom labeling scheme is depicted in Figure 3. Standard deviations are given.

complexes **I3a** and **I3b** (in which the OH ligand of **I2a** and **I2b** is replaced by an ammonia ligand). In **I3a** the ionicity of the N(3)−N(2) bond increases by $\Delta BI_{N(3)-N(2)} = +0.08$ and +0.06 with respect to **I2a**, while an opposite trend is observed for **I3b**, in which the ionicity of the N(3)−N(2) bond decreases by $\Delta BI_{N(3)-N(2)} = -0.03$ and −0.01. Thus, the bonding situation becomes similar to **4** and **5** ($\Delta BI_{N(3)-N(2)} = -0.04$ and −0.00 for **I3a** with respect to **4** and $\Delta BI_{N(3)-N(2)} = +0.01$ and +0.00 for **I3b** with respect to **5**), and this translates in a similar ΔE of isomerization of ∼17 kcal/mol.

3.2. Hybrid QM/MM Molecular Dynamics Simulations of the Drug−DNA Adducts. A QM/MM simulation of **1** in complex with d(CpTpCpTpG*pG*pTpCpTpCp) (**A**) was first carried out to establish the accuracy of our computational method by direct comparison with the NMR data.[12] Then, we have followed the dynamics of **2** in complex with the same oligonucleotide (**B**), in the same binding mode of **A**, and finally we have carried out a simulation of the migration product of **2** bound to the same oligonucleotide (**C**). For the two latter adducts no NMR structure is available; therefore a comparison among the three simulations provides a detailed description of the changes at the local geometry of the d(GpG) binding site induced by the diazole-bridged diplatinum drugs.[43] The classically equilibrated geometries were used as starting structures to perform ∼5 ps of QM(Car−Parrinello)/MM MD simulations at ∼300 K for **A**−**C**.

3.2.1. Complex A. The QM/MM simulation suggests that the coordination geometry of the two metallic centers is rather symmetric (Table 3). The average structural parameters of the two coordination spheres are practically identical. As in the gas phase models, the BLYP functional slightly overestimates the bond lengths with respect to the NMR structure, with the largest error of $\Delta d \approx 0.05$ Å (2% relative error).

In contrast to **1** in the gas phase, **A** presents identical Pt−$NH_{3\ cis}$ and Pt−$NH_{3\ trans}$ bond lengths, because of the presence of the macromolecular environment and the solvent. However, in **A** the two $NH_{3\ cis}$ ligands are not equivalent: While both $NH_{3\ cis}$ ligands form intramolecular hydrogen bonds with O(6)@G5,6 ($NH_{3\ cis}$···O(6)@G5,6 = 2.1 ± 0.4 Å and 2.0 ± 0.1 Å, respectively), $NH_{3\ cis}$ bound to Pt(2) forms an additional hydrogen bond with O(4)@T7 ($NH_{3\ cis}$@Pt(2)···O(4)@T7 = 2.0 ± 0.1 Å) (Figure 4a and Table 4). In contrast, the $NH_{3\ cis}$@Pt-(1), although within a reasonable distance of 2.1 ± 0.4 Å, does not form a hydrogen bond with O(4)@T4, because of the geometric constraints imposed by the DNA. In addition, small differences are observed in the hydration sphere of corresponding NH_3 ligands, with the $NH_{3\ trans}$ ligands being more solvent exposed (∼2.6, 2.9 vs ∼4.1, 4.5 within the first 3.3 Å from the ammonia nitrogen, for $NH_{3\ cis}$@Pt(1,2) and $NH_{3\ trans}$@Pt(1,2), respectively, Table 5).

TABLE 4: Selected Hydrogen Bond Distances (Å) between the Ammonia Ligands and G5, T4, G6, and T7 of A−C[a]

hydrogen bonds (Å)	NMR	A	B	C
Pt(1)@$NH_{3\ cis}$···O(6)@G5	2.3	2.1 ± 0.4	1.9 ± 0.2	
	2.9	*2.8 ± 0.4*	*2.8 ± 0.1*	
		(73%)	(100%)	
Pt(1)@$NH_{3\ cis}$···O(4)@T4	2.0			1.9 ± 0.1
	3.1			*2.9 ± 0.1*
				(100%)
Pt(2)@$NH_{3\ cis}$···O(6)@G6	2.6	2.0 ± 0.1		
	2.9	*3.0 ± 0.1*		
		(94%)		
Pt(2)@$NH_{3\ cis}$···O(4)@T7	2.5	1.9 ± 0.1	1.9 ± 0.1	1.9 ± 0.1
	3.1	*2.8 ± 0.1*	*2.8 ± 0.1*	*2.9 ± 0.1*
		(89%)	(100%)	(100%)

[a] Average donor−acceptor distances are given in italic, while persistence of the hydrogen bonds is given in parentheses.

TABLE 5: Average Number of Water Molecules within the First Coordination Shell of NH_3 Ligands (within a Distance of 3.3 Å from the N Atom of the Ammonia Ligands)

	A	B	C
Pt(1)$NH_{3\ trans}$	4.1	5.2	3.8
Pt(1)$NH_{3\ cis}$	2.6	2.1	2.6
Pt(2)$NH_{3\ trans}$	4.5	5.0	5.3
Pt(2)$NH_{3\ cis}$	2.9	3.9	2.7

The platinated moiety is well reproduced (average root-mean-square deviation of ∼0.6 Å relative to the NMR structure). Visual inspection of the superposition of the average QM/MM structure and the NMR structure confirms that the structural agreement is remarkable (Figure 6). The observed discrepancies are mainly due to fluctuations of the pyrazolate unit (with respect to the plane going through the $NH_{3\ trans}$ ligands and the two Pt atoms, Figure 6) and the rotation of the ammonia ligands. The root-mean-square deviation of the entire DNA is larger (∼1.4 Å), and it is mainly given by the deviation between the initial classically equilibrated structure and the NMR structure.[44]

Due to the limited time scale of our QM/MM simulations the only relevant comparison concerns local parameters of the platinated moiety. To give an accurate description of global DNA parameters, extensive classical molecular dynamics simulations are required using accurate parameters for the platinum coordination site. [43,45]

However, the local structural parameters of the platinated bases, G5−G6, are in good agreement with the NMR structure (Table 6). The rise of the calculated structure is larger by +0.3 Å. This could be due to the DFT method, which neglects the dispersion interactions between π-stacked aromatic rings.[41] Consequently, the roll angle is higher than that found experimentally (+5°), whereas the tilt angle is slightly smaller (−2°). As a result, the angle between the two platinated bases is slightly higher (+4°) compared to the NMR structure. However, in contrast to cisplatin this drug does not induce any global kink in duplex DNA.[19,46] The propeller twists of the G5−C16 and G6−C15 base pairs are larger in **A** with respect to the NMR structure. The discrepancy arises mainly from a rearrangement of the C15 and C16 bases on the strand opposite to the platinated moiety (Figure 6).

Comparison to the free oligonucleotide, equilibrated by classical MD simulation, allows us to define the extent of the

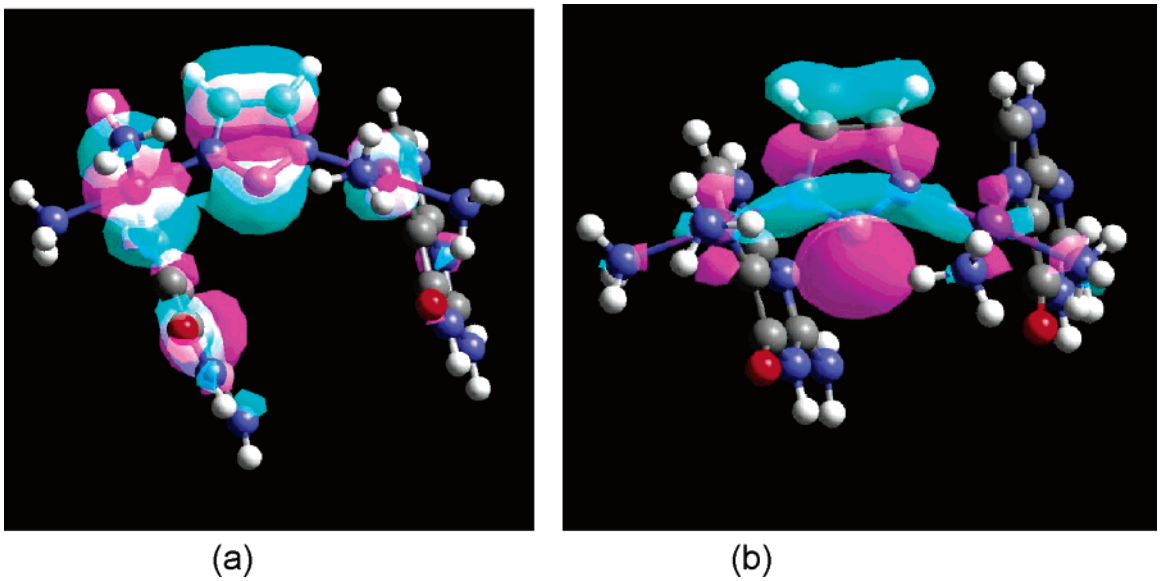

Figure 5. One-electron Kohn−Sham orbitals of $[\{cis\text{-}Pt(NH_3)_2\}_2(G)_2(\mu\text{-}1,2,3\text{-}ta\text{-}N(1),N(3))]^{3+}$ (with ta = 1,2,3-triazolate) (a) HOMO-15 and (b) HOMO-20. Contours are drawn at ±5 a.u.

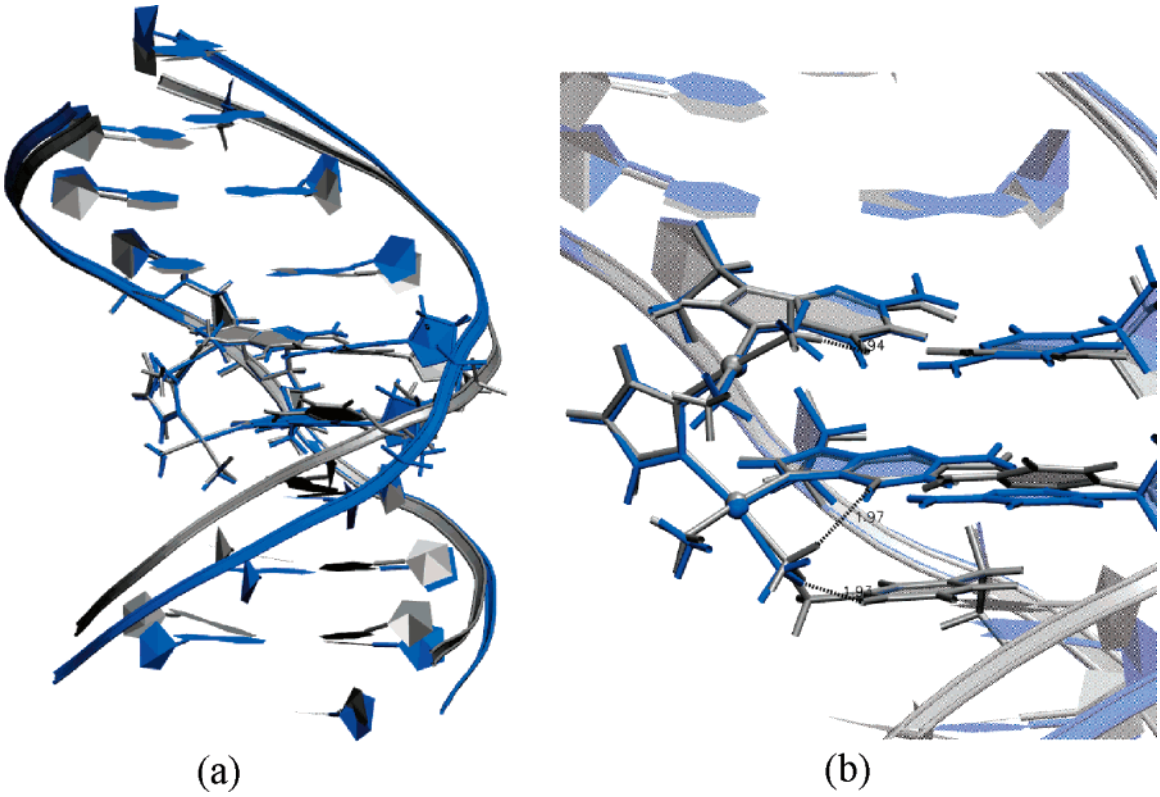

Figure 6. (a) Overlap of the NMR structure (blue) and the average QM/MM structure of **A** (silver). (b) Close view of the platinated site, with hydrogen bonds between $NH_{3\,cis}$ to guanine and thymine bases indicated by dashed black lines.

distortions induced by the drug on ds DNA, and it reveals some interesting differences. Both roll and tilt angles at the G5−G6 step increase by +12° with respect to the free oligonucleotide. In the uncomplexed DNA, the G5−G6 step is much less distorted, with roll and tilt angles close to 0°, and also the rise adopts a value close to standard B-DNA. On the other hand, the twist at the G5−G6 step diminishes by −8° from 39° in free DNA to 31° in **A**, indicating a local unwinding of the double helix at the platinated step.

3.2.2. Complex B. In this complex, only the nature of the bridging unit is changed with respect to **A**. Pt(1) and Pt(2) are however still coordinated to N(1) and N(2) of the triazolate, respectively, as in **A** (Figure 4b). Therefore, we expect the local structural distortions that the drug induces to the ds DNA to be very similar to **A**.

Indeed, the coordination spheres of the two metallic centers are symmetric as in **A** and present structural parameters identical to **A**. However, the distance between the two Pt atoms slightly increases to 4.1 ± 0.1 Å (+0.03 Å with respect to **A**).

Also in **B** intramolecular hydrogen bonds are observed between the cis ammonia ligands and the biomolecular frame: $NH_{3\,cis}$ coordinated to Pt(1) forms an intramolecular hydrogen

TABLE 6: Selected Structural Parameters for the Free DNA, the NMR Structure, and the Three QM/MM Simulations (A, B, and C)[a]

	free DNA	NMR	**A**	**B**	**C**
roll G5−G6	−3 ± 7	5	9 ± 4	4 ± 4	−5 ± 5
twist G5−G6	39 ± 4	29	31 ± 2	32 ± 3	35 ± 3
tilt G5−G6	−4 ± 5	10	8 ± 3	8 ± 3	18 ± 4
rise G5−G6	3.4 ± 0.2	3.3	3.6 ± 0.2	3.6 ± 0.2	4.1 ± 0.3
propeller twist G5−C16	−2 ± 7	−12	−18 ± 4	−22 ± 7	−8 ± 5
propeller twist G6-C15	−15 ± 7	−13	−22 ± 5	−11 ± 5	−3 ± 6
angle G5−G6	4 ± 2	3	7 ± 2	4 ± 1	6 ± 1
overall axis bend	19 ± 8	5	19 ± 5	10 ± 3	8 ± 4

[a] Angles (twist, tilt, propeller twist, and roll) and axis bend[46] are given in degrees, while rise is given in angstroms. The angles[34] (degrees) between G5 and G6 of the ds DNA are also given.

bond with O(6)@G5 ($NH_{3\,cis}$@Pt(1)···O(6)@G5 = 1.9 ± 0.2 Å), while $NH_{3\,cis}$ coordinated to Pt(2) forms a hydrogen bond with O(4)@T7 ($NH_{3\,cis}$@Pt(2)···O(4)@T7 = 1.9 ± 0.1 Å).

Both the cis and the trans ammonia ligands are more water exposed than those in **A** (Figure 4b) as indicated by the average numbers of water molecules that lie in the first coordination shell (i.e., 2.1, 3.9 and 5.2, 5.0 for $NH_{3\,cis}$@Pt(1,2) and for $NH_{3\,trans}$@Pt(1,2), respectively, Table 5). The asymmetric hydration of both the cis and the trans ammonia ligands might be due to a slight perturbation provoked by N(3) of the triazolate ring. The latter is a weak hydrogen bond donor with its own solvation shell (2.5 waters). As a result, the platinated moiety of **B** is slightly more hydrated than that in **A**.

The rise of the G5−G6 base step along with the tilt and the twist angles are identical to **A**, and they are not affected by the presence of the triazolate unit. A decrease of the roll angle between G5 and G6 (−5° with respect to **A**) is observed, while the angle between the two guanine bases is the same as that in the free oligonucleotide, and it is close to 0° as in canonical B-DNA.

A decrease (−4°) of the propeller twist is observed for the G6−C15 base pair, while for the G5−C16 base pair this angle increases by +11°. In conclusion, the local structural parameters of **B** are very similar to those of **A**.

3.2.3. Complex C. This simulation describes the changes of the local geometry of the d(GpG) binding site as a function of the coordination mode of **2**.

Both of the Pt(1,2)−N(1,3) distances slightly decrease relative to **A** and **B**, while all of the other coordination bonds remain identical. However, in agreement with the formation of an allylic structure (already observed in **5**) the two N(1)−N(2) and N(2)−N(3) bonds become equivalent. Inspection of the Kohn−Sham orbitals confirms this hypothesis, showing a molecular orbital involving the three nitrogens of the triazolate ring along with the presence of an electronic correlation between the two metallic centers mediated by the allylic moiety (similar to that shown in Figure 3b). This confirms that the formation of **C** is driven by the thermodynamic stabilization due to the formation of an allylic isomer.

Intramolecular hydrogen bonds stabilize the drug−DNA adduct. Both of the cis ammonia ligands form hydrogen bonds to O(4)@T4,7 ($NH_{3\,cis}$@Pt(1,2)···O(4)@T4,7 = 1.9 ± 0.1 Å). As already observed for **B**, the diplatinated drug is slightly more hydrated than in **A** (average number of water molecules ∼2.6, 2.7 and 3.8, 5.3 for the $NH_{3\,cis}$@Pt(1,2) and $NH_{3\,trans}$@Pt(1,2) ligands, respectively).

In **C**, the rise of the G5−G6 base step increases (4.1 ± 0.3 Å, +0.5 Å relative to **A**, Table 6). This value is now larger by +0.7 Å than that in free DNA, and it reaches the value of the rise of cisplatin−DNA adducts.[15] Interestingly, the rise is identical in **A** and **B**, and it increases substantially in **C**.

The roll angle of the G5−G6 base pair decreases by −9° relative to **B,** while the tilt angle of the same base pair increases by +10°, leading to an opening of the two bases and causing the large rise. The angle between the guanine bases arises from a combination of nonzero roll and tilt angles.[34] Given the decrease of the roll angle and the increase of the tilt angle, passing from **A** to **C**, the resulting angle between the two platinated base pairs fluctuates around an almost constant value.

The twist angle, which is rather low in **A** and **B**, increases in **C**, approaching the value typical of canonical B-DNA. This could be due to the expansion of the linking unit (which possesses four atoms in **A** and **B** and five atoms in **C**) that confers higher flexibility to the G5−G6 step, leading to a relaxation of the twist angle.

Also the propeller twists of the G5−C16 and G6−C15 base pairs increase by +14° and +8°, respectively, and for G5−C16 this angle becomes closer to that of the free oligonucleotide.

In conclusion, we observe clear trends in most structural parameters describing the platinated base pair when going from **A** to **C**. The roll angle shows a remarkable reduction, while the tilt angle doubles. This leads to a substantial increase of the rise between the two base pairs, which is similar to the one observed for the cisplatin−DNA adduct.[15] However, the nature of the distortion is quite different as well as the effect of the local distortion on the global DNA structure: In the cisplatin−DNA adduct, the separation of the platinated guanines is mainly caused by a large positive roll,[15] while in the dinuclear Pt−DNA complexes the separation of the guanines is mainly due to an increase of the tilt. This leads in cisplatin to a large kink toward the major groove, while in the dinuclear Pt−DNA adducts the angle (and consequently the kink) between the platinated base pairs remains small. Indeed, the scaffold of the dinuclear drug has been especially designed to prevent large distortions in the DNA, using two metallic centers that are separated by the typical interbase distance of B-DNA.

As already proven experimentally for **A**, our simulations allow us to state that also in **B** and **C** the distortion of the double helix is much lower than that typically induced by cisplatin.[15,46] In addition, a relative comparison among the three models is very interesting and could help to establish a correlation between distortion and cytotoxicity of different Pt compounds.

Conclusions

We have presented structural and electronic properties of a novel generation of dinuclear azole-bridged platinum complexes **1** and **2**, containing pyrazolate and triazolate bridging units, respectively.

For **2** a significant thermodynamic stabilization (by −10 and −20 kcal/mol for the intermediate (**I2b**) and the product (**5**), respectively (Figure 2)) comes along with the isomerization mechanism of the Pt(2) coordination sphere from N(2) to N(3). This thermodynamic stabilization is caused by the formation of an allylic complex involving the three nitrogen atoms of the triazolate unit.

The average QM/MM structure of the **1**−DNA adduct (**A**) compares well with the NMR structure. QM/MM simulations of the related triazolate compounds **2** (bound to DNA in N(1),-N(2) and N(1),N(3) fashions, **B** and **C**, respectively) reveal the following trends: (i) a decrease in the roll angle of the platinated

G5−G6 bases when going from **A** to **C**, (ii) an increase of the rise at the platinated G5−G6 base step that in **C** becomes comparable to that observed in cisplatin−DNA adducts[15] (in contrast to cisplatin, the large rise does not come along with an increase in curvature of ds DNA, an unwinding of the double helix, and a compression of the major groove),[15,46] (iii) a constant value of the tilt in **A** and **B** and a large increase in **C** (these two parameters partially compensate each other, such that the angle between the two base pairs[34] remains small in all three systems and it does not produce any global kink in the DNA),[15] (iv) a small overall axis bend is observed for **A**−**C**.[46]

The absence of the kink and a small axis bend may render the platinated lesion less recognizable to the NER enzymes, working around the problem of cellular resistance.[5]

Our results based on QM/MM simulations provide a description of local distortions at the platinated site, but for a detailed picture of the global distortions in DNA classical MD simulations on a longer time scale would be required.[43,45,46] To this end, the results of the QM/MM simulations will be helpful in a reassessment of the force field parameters for such metal-containing systems to perform extensive classical molecular dynamics simulations.[43,45]

In conclusion, our findings complement the available experimental data to understand the mechanism of action of platinum anticancer agents still under debate, and they may be crucial for the development of more specific anticancer complexes.

Acknowledgment. We thank P. Melis (Cagliari) and A. Vargiu (SISSA) for their contribution in the preliminary phase of the project. One of the authors (J.R.) is grateful to two former Ph.D. students, S. Komeda and J. M. Teuben, for collection of experiments in their projects that led to the preliminary structure of the DNA adduct with compound **1**. Computational resources have been granted by CINECA (INFM Grants) and CASPUR (CNR-INFM SLACS). The authors thank the COST organization for financial support.

References and Notes

(1) (a) Reedijk, J. New clues for platinum antitumor chemistry: Kinetically controlled metal binding to DNA. *Proc. Natl. Acad. Sci. U.S.A.* **2003**, *100*, 3611. (b) Wang, D.; Lippard, S. J. Cellular processing of platinum anticancer drugs. *Nat. Rev. Drug Discovery* **2005**, *4*, 307.

(2) Wong, E.; Giandomenico, C. M. Current status of platinum-based antitumor drugs. *Chem. Rev.* **1999**, *99*, 2451.

(3) Reedijk, J. Why does cisplatin reach guanine-N7 with competing S-donor ligands available in the cell? *Chem. Rev.* **1999**, *99*, 2499−2510.

(4) Jamieson, E. R.; Lippard, S. J. Structure, recognition, and processing of cisplatin−DNA adducts. *Chem. Rev.* **1999**, *99*, 2467−2498.

(5) Zorbas, H.; Keppler, K. Cisplatin Damage: Are DNA Repair Proteins Saviors or Traitors to the Cell? *ChemBioChem* **2005**, *6*, 1157.

(6) Reedijk, J. Medicinal applications of heavy-metal compounds. *Curr. Opin. Chem. Biol.* **1999**, *3*, 236−240.

(7) Jakupec, M. A.; Galaski, M.; Keppler, B. K. Tumour-inhibiting platinum complexes−State of the art and future perspectives. *Rev. Physiol. Pharmacol.* **2003**, *146*, 1−54.

(8) Komeda, S.; Lutz, M.; Spek, A. L.; Chikuma, M.; Reedijk, J. New antitumor-active azole-bridged dinuclear platinum(II) complexes: Synthesis, characterization, crystal structures, and cytotoxic studies. *Inorg. Chem.* **2000**, *39*, 4230−4236.

(9) Komeda, S.; Ohishi, H.; Yamane, H.; Harikawa, M.; Sakaguchi, K.; Chikuma, M. An NMR study and crystal structure of [{*cis*-Pt(NH_3)$_2$-(9EtG-κN7)}$_2$-(μ-pz)][NO_3]$_3$ (9EtG = 9-ethylguanine) as a model compound for the 1,2-intrastrand GG crosslink. *J. Chem. Soc., Dalton Trans.* **1999**, *17*, 2959−2962.

(10) (a) Komeda, S.; Bombard, S.; Perrier, S.; Reedijk, J.; Kozelka, J. Kinetic study of azole-bridged dinuclear platinum(II) complexes reacting with a hairpin-stabilized double-stranded oligonucleotide. *J. Inorg. Biochem.* **2003**, *96*, 357−366. (b) Komeda, S.; Yamane, H.; Chikuma, M.; Reedijk, J. A kinetic study on the reactions of azolato-bridged dinuclear platinum-(II) complexes with guanosine 5′-monophosphate. *Eur. J. Inorg. Chem.* **2004**, *24*, 4828−4835.

(11) Komeda, S.; Lutz, M.; Spek, A. L.; Yamanaka, Y.; Sato, T.; Chikuma, M.; Reedijk, J. A novel isomerization on interaction of antitumor-active azole-bridged dinuclear platinum (II) complexes with 9-ethylguanine. Platinum(II) atom migration from N2 to N3 on 1,2,3-triazole. *J. Am. Chem. Soc.* **2002**, *124*, 4738−4746.

(12) Telechtea, S.; Komeda, S.; Teuben, J. M.; Elizondo-Riojas, M. A.; Reedijk, J.; Kozelka, J. A pyrazolate-bridged dinuclear platinum(II) complex induces only minor distortions upon DNA-binding. *Chem.−Eur. J.*, in press.

(13) Laio, A.; VandeVondele, J.; Rothlisberger, U. A Hamiltonian electrostatic coupling scheme for hybrid Car−Parrinello molecular dynamics simulations. *J. Chem. Phys.* **2002**, *116*, 6941−6947.

(14) Carloni, P.; Rothlisberger, U.; Parrinello, M. The role and perspective of ab initio molecular dynamics in the study of biological systems. *Acc. Chem. Res.* **2002**, *35*, 455−464.

(15) Spiegel, K.; Rothlisberger, U.; Carloni, P. Cisplatin binding to DNA oligomers from hybrid Car−Parrinello/molecular dynamics simulations. *J. Phys. Chem. B* **2004**, *108*, 2699−2707.

(16) Hutter, J.; Alavi, A.; Deutsch, T.; Ballone, P.; Bernasconi, M.; Focher, P.; Goedecker, S. *CPMD*; Max-Planck-Institut für Festkörperforschung, IBM Research: Stuttgart, Germany, 1995−1999.

(17) Trouiller, N.; Martins, J. L. Efficient pseudopotentials for plane-wave calculation. *Phys. Rev. B* **1991**, *43*, 1993−2006.

(18) Kleinman, L.; Bylander, D. M. Efficacious form for model pseudopotentials. *Phys. Rev. Lett.* **1982**, *48*, 1425−1428.

(19) Becke, A. D. Density-functional exchange-energy approximation with correct asymptotic behavior. *Phys. Rev. A* **1998**, *38*, 3098−3100.

(20) Lee, C.; Yang, W.; Parr, R. G. Development of the Colle−Salvetti correlation-energy formula into a functional of the electron density. *Phys. Rev. B* **1988**, *37*, 785−789

(21) Barnett, R. N.; Landman, U. Born−Oppenheimer molecular-dynamics simulations of finite systems: Structure and dynamics of $(H_2O)_2$. *Phys. Rev. B* **1993**, *48*, 2081−2097.

(22) Case, D. A.; Pearlman, D. A.; Caldwell, J. W.; Cheathman, T. E., III; Ross, W. S.; Simmerling, C. L.; Darden, T. A.; Merz, K. M.; Stanton, R. V.; Cheng, A. L.; Vincent, J. J.; Crowley, M.; Tsui, V.; Radner, R. J.; Duan, Y.; Pitera, J.; Massova, I.; Seibel, G. L.; Singh, U. C.; Weiner, P. K.; Kollman, P. A. *AMBER*, version 7; University of California: San Francisco, 2002.

(23) Pearlman, D. A.; Case, D. A.; Caldwell, J. W.; Ross, W. S.; Cheatham, T. E., III; DeBolt, S.; Ferguson, D.; Seibel, G. L.; Kollman, P. A. AMBER, A package of computer programs for applying molecular mechanics, normal-mode analysis, molecular dynamics and free energy calculations to simulate the structural and energetic properties of molecules. *Comput. Phys. Commun.* **1995**, *91*, 1−41.

(24) Cornell, W. D.; Cieplak, P.; Bayly, C. I.; Gould, I. R.; Merz, K. M., Jr.; Ferguson, D. M.; Spellmeyer, D. C.; Fox, T.; Caldwell, J. W.; Kollman, P. A. A second generation force field for the simulation of proteins, nucleic acids, and organic molecules. *J. Am. Chem. Soc.* **1995**, *117*, 5179−5197.

(25) Cheatham, T. E., III; Cieplak, P.; Kollman, P. A. A modified version of the Cornell et al. force field with improved sugar pucker phases and helical repeat. *J. Biomol. Struct. Dyn.* **1999**, *16*, 845−862.

(26) Joergensen, W. L.; Chandrasekhar, J.; Madura, J. D.; Impey, R. W.; Klein, M. L. Comparison of simple potential functions for simulating liquid water. *J. Chem. Phys.* **1983**, *79*, 926−935.

(27) Herman, F.; Kozelka, J.; Stoven, V.; Guittet, E.; Girault, J. P.; Huynh-Dinh, T.; Igolen, J.; Lallemand, J. Y.; Chottard, J. C. A d(GpG)-platinated decanucleotide duplex is kinked. An extended NMR and molecular mechanics study. *Eur. J. Biochem.* **1990**, *194*, 119−133.

(28) Cheatham, T. E., III; Miller, J. L.; Fox, T.; Darden, T. A.; Kollman, P. A. Molecular dynamics simulations on solvated biomolecular systems: The Particle mesh Ewald method leads to stable trajectories of DNA, RNA, and proteins. *J. Am. Chem. Soc.* **1995**, *117*, 4193−4194.

(29) Berendsen, H. J. C.; Postma, J. P. M.; van Gunsteren, W. F.; DiNola, A.; Haak J. R. Molecular dynamics with coupling to an external bath. *J. Chem. Phys.* **1984**, *81*, 3684−3690.

(30) van Gunsteren W. F. *Biomolecular Simulation: The GROMOS96 Manual and User Guide*; Hochschulverlag AG der ETH Zuerich: Zuerich, Switzerland, 1996.

(31) Laio, A.; VandeVondele, J.; Rothlisberger, U. D.-RESP: Dynamically generated electrostatic potential derived charges from quantum mechanics/molecular mechanics simulations. *J. Phys. Chem. B* **2002**, *106*, 7300−7307.

(32) Nose, S. J. *J. Chem. Phys.* **1984**, *81*, 511−519.

(33) Hoover, W. G. *Phys. Rev. A* **1985**, *31*, 1695−1697.

(34) This angle refers to the angle between the normal vectors onto the best plane describing the base pair under consideration

(35) Dickerson, R. E. Definitions and nomenclature of nucleic acid structure parameters. *J. Biomol. Struct. Dyn.* **1989**, *6*, 627−634.

(36) Lavery, R.; Sklenar, H. Defining the structure of irregular nucleic acids−Conventions and principles. *J. Biomol. Struct. Dyn.* **1989**, *6*, 655−667

(37) Marzari, N.; Vanderbilt, D. Maximally localized generalized Wannier functions for composite energy bands. *Phys. Rev. B.* **1997**, *56*, 12847−12865.

(38) Alber, F.; Folkers, G.; Carloni, P. Dimethyl phosphate: Stereoelectronic versus environmental effects. *J. Phys. Chem. B* **1999**, *103*, 6121−6126.

(39) Carloni, P.; Andreoni, W.; Hutter, J.; Curioni, A.; Giannozzi, P.; Parrinello, M. Structure and bonding in cisplatin and other Pt(II) complexes. *Chem. Phys. Lett.* **1995**, *234*, 50.

(40) We consider the distance between the centers of the C−C bond connecting the two aromatic rings of the guanine bases.

(41) The discrepancy of ∼0.3 Å observed in the base step is attributable to the well-known deficiency of DFT in correctly reproducing π-stacking interactions. (Kristyan, S.; Pulay, P. Can (semi)local density functional theory account for the London dispersion forces? *Chem. Phys. Lett.* **1994**, *229*, 175−180.) The lack of dispersion interactions in DFT typically leads to an opening of π-stacking aromatic rings. (Magistrato, A.; Merlin, M.; Albinati, A.; Pregosin, P. S.; Rothlisberger, U. Electronically and sterically induced structural distortions in square-planar d^8 complexes. *Organometallics* **2000**, *19*, 3591−3596. Magistrato, A.; Pregosin, P. S.; Albinati, A.; Rothlisberger, U. The role of $\pi-\pi$ stacking interactions in organometallic compounds. Combined quantum mechanics/molecular mechanics studies. *Organometallics* **2001**, *20*, 4178−4184.)

(42) By definition, the maximally localized Wannier functions are not suited to describe strongly delocalized bonds (ref 38). However, we believe that a relative comparison of the bond ionicity of the reaction intermediates and the products is useful for a qualitative understanding of their bonding.

(43) These structural changes are clearly limited by the time scale of our simulation (a few picoseconds only). At the present we can perform an analysis of local parameters of the platinated complex, while longer scale molecular dynamics simulations are required to obtain converged global parameters.

(44) The final classical MD structures have a root-mean-square deviation of ∼1.4 Å with respect to the initial NMR structure.

(45) (a) Ercolessi, F. *Europhys. Lett.* **1994**, *26*, 583. (b) Maurer, P. First-principles characterization of radiopharmaceuticals and steps towards der rational design. Ph.D. Dissertation 15316, ETH Zurich (Switzerland), 2004; Chapter 5, pp 121−150. (c) Maurer, P.; Laio, A.; Rothlisberger, U. On-the-fly parametrization of classical force field from QM/MM simulations, to be submitted for publication.

(46) A relative comparison of the axis bends of the three structures may also be meaningful. As already observed for cisplatin,[15] a simulation of a few picoseconds may already point out if relevant structural changes will occur upon binding of the drug. A decrease of the overall axis bend passing from **A** to **C,** although not relevant in absolute value, is an indication that, in contrast to cisplatin, these drugs may cause a release of the overall axis bend.